Interfacial Kinetics in a Model Emulsion Polymerisation System Using Microelectrochemical Measurements at Expanding Droplets (MEMED) and Time Lapse Microscopy

Elizabeth E. Oseland,[†] Anita Rea,[‡] Martine de Heer,[‡] Jeffrey Fowler,[‡] and Patrick R. Unwin*[,†]

[†]*Department of Chemistry, University of Warwick, Coventry CV4 7AL, United Kingdom*

[‡]*Jealott's Hill International Research Centre, Bracknell, Berkshire RG42 6EY, United Kingdom*

* Corresponding author

*E-mail address: p.r.unwin@warwick.ac.uk (P. R. Unwin), Telephone: +44 24 76524112

Abbreviations: MEMED, microelectrochemical measurements at expanding droplets; PMPs, polymeric micro particles; AI, active ingredient; FT-IR, Fourier transform infrared spectroscopy; IrOx, iridium oxide; RDGE, resorcinol diglycidyl ether; OCP, open circuit potential; FEM, finite element method;

Abstract

Physicochemical processes that take place at the oil-water interface of an epoxy-amine emulsion polymerisation system influence the properties and structural morphology of the polymeric microparticles formed. Investigating these processes, such as the transport of monomers across the liquid/liquid interface brings new understanding which can be used to tune polymeric morphology. Two different approaches are used to provide new insights on these processes. Microelectrochemical measurements at expanding droplets (MEMED) are used to measure the transfer of amine from an organic phase comprised of epoxide and amine into an aqueous receptor phase. The rate of amine transfer across the liquid/liquid interface is characterised using MEMED and finite element method modelling and kinetic values are reported. Time lapse microscopy of epoxide droplets held in deionised water or an aqueous amine solution heated to different temperatures is further used to characterise epoxide dissolution into the aqueous phase. Mass-transport of epoxide into the aqueous phase is shown to be temperature-dependent. Epoxide homopolymerisation at the droplet-water interface is found to influence the rate of epoxide droplet dissolution. The rate of the epoxy-amine cure reaction is shown to be faster than the rate of the epoxide homopolymerisation reaction.

Keywords: Interfacial polymerisation, Liquid/liquid interface, Microelectrochemical measurements at expanding droplets (MEMED), Finite element method modelling (FEM), Epoxide-amine, Time-lapse microscopy

Introduction

Reactions that take place at an immiscible liquid/liquid interface are prevalent across a wide variety of systems, from the biological to the industrial.[1] One such process is the emulsion polymerisation, whereby chemical monomers polymerise at an immiscible liquid/liquid interface to form polymeric microparticles (PMPs). PMPs can be incorporated into useful products such as paints[2], coatings[3] and adhesives.[4] There is also interest in exploiting the morphology of PMPs to encapsulate and controllably release active ingredients (AIs) such as drugs[5], vaccines[6], or agrochemicals.[7] The release of an AI from within a PMP can be achieved either by diffusion of the AI through the PMP wall[8] or by breakdown of the PMP wall, with the latter providing a higher level of control if the PMP has been designed to degrade when it comes into contact with certain stimuli such as a change in pH[5] or temperature.[9] Henceforth, the rate at which AI is released will be influenced by PMP morphology.

One method of PMP fabrication is the temperature-dependent addition reaction between an epoxide and an amine, represented in Scheme 1.

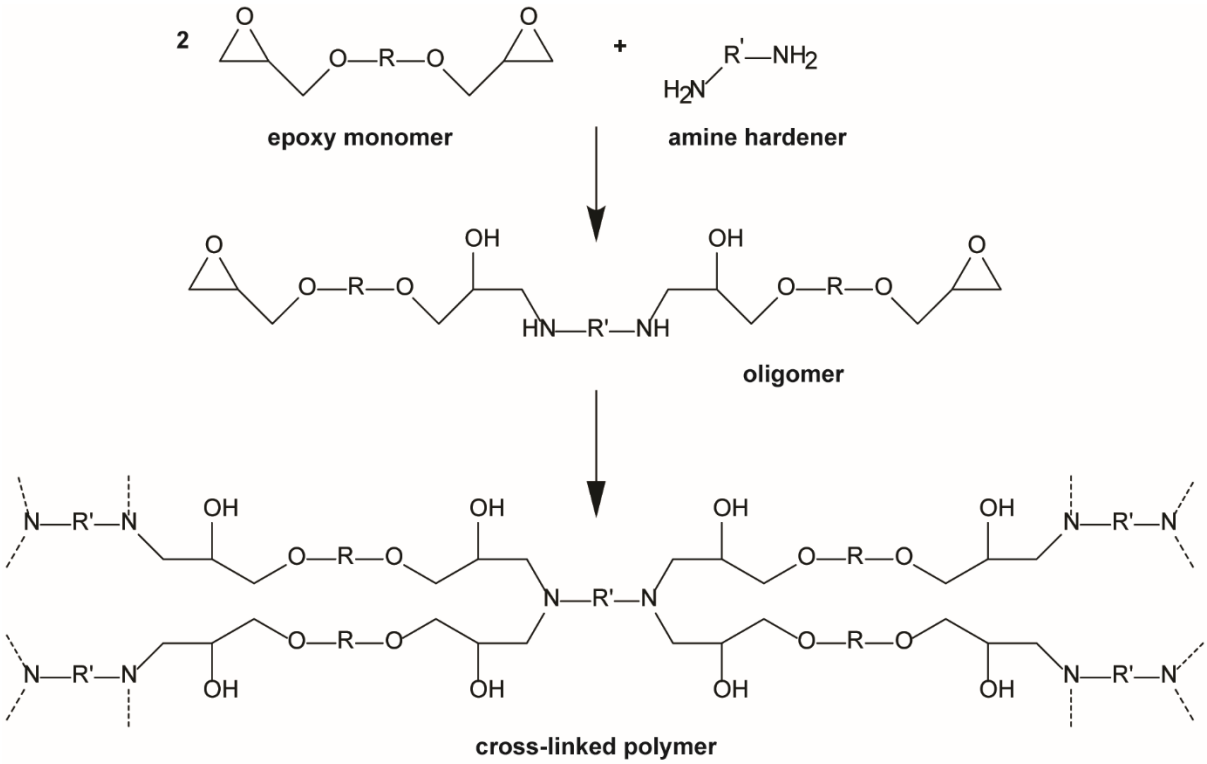

Scheme 1. The temperature dependent addition reaction between an epoxide and an amine to form a cross-linked epoxy polymer. Active ingredient (AI) is typically dispersed in the organic phase containing both epoxide monomer and amine hardener. This is then dispersed via sonication in an aqueous continuous phase containing kaolin clay and surfactants to stop droplets from coalescing.[10] The solution is then heated to initiate the epoxy-amine polymerisation reaction, with the interface between the organic dispersed phase and the aqueous continuous phase ensuring that the curing process forms spherical PMPs embedded with AI.

Figure 1 shows a conceptual model of an epoxy-amine droplet within the aqueous phase, with particles of kaolin clay at the liquid-liquid interface. Whilst the curing reaction is expected to take place in the organic phase, monomer transfer into the aqueous phase will lead to enhanced curing at the liquid-liquid interface or in the aqueous phase itself. Therefore, to fully understand epoxy-amine PMP formation, cure kinetics in both phases and the extent

of monomer transfer need to be quantified. Implementation of analytical techniques capable of describing these processes is highly desirable to ensure effective industrial scale up of epoxy-amine emulsion polymerisation technology.

Cure kinetics in the organic phase have previously been studied using a variety analytical techniques. Fourier transform infra-red (FT-IR) spectroscopy and isothermal differential scanning calorimetry (DSC) have been used to measure cure kinetics of epoxy-amine mixtures at different temperatures, with higher temperatures causing faster curing kinetics.[11, 12] Activation energies for epoxy-amine cure systems have been extracted using the Kamal equation from DSC kinetic data.[13] High-performance liquid chromatography (HPLC) has also been used to study how changing the amine-to-epoxide ratio can affect the progress of a curing reaction.[14] This particular study, using a model system of phenyl glycidyl ether, the curing agent *p*-chloroaniline and the accelerator Monuron, showed that catalysed amine curing of epoxy resins is controlled by a competition between epoxy homopolymerisation and amine addition to the epoxy. This competition is influenced by the ratio of epoxy-to-amine, catalyst concentration and temperature.

Studies into epoxy-amine cure kinetics in the presence of water are less widespread, however there are examples in the literature. Initial studies into the effect of absorbed water on undercured epoxy-amine thermosets indicated that additional curing would take place in the presence of hot water.[15, 16] This is due to a reaction between unreacted epoxide and water. More recently, Choi *et al.* have used FT-IR to quantify the cure kinetics of an epoxy-amine thermoset in the presence of different amounts of water.[17]

Figure 1. A conceptual model of the polymeric microparticle (PMP) curing process which shows amine and epoxide monomer transfer across the oil-water interface and the location of the epoxy-amine curing reaction.

Although the analytical techniques mentioned are of great value when probing the cure kinetics of epoxy-amine thermosets, they cannot sufficiently describe monomer transfer or curing taking place at the liquid-liquid interface. Information regarding these processes will provide insight into the position of the curing reaction (i.e. does it take place in the organic phase or the aqueous phase?), which influences the morphology.

Microelectrochemical measurements at expanding droplets (MEMED) is a technique that has been shown to be powerful for quantifying the chemical processes that take place at a liquid/liquid interface.[18-24] It employs either amperometric or potentiometric detection to measure local changes in concentration as a droplet expands towards a stationary microelectrode placed in an immiscible receptor liquid phase. MEMED has previously been used to investigate stripping kinetics and electron transfer at oil-water interfaces, as well as the characterisation of mass-transport in both the oil and aqueous phases.[20, 24] Mass-transport models can be generated which use the convective-diffusion equation and appropriate boundary conditions to generate theoretical concentration profiles which can be used to quantify chemical fluxes at the liquid/liquid interface.[20, 25]

The dissolution of a liquid droplet into a receptor liquid can also be characterised using optical techniques. Needham *et al.* have used a calibrated video micrograph to measure the dissolution of aniline droplets into water and vice-versa as a function of solution saturation.[26] The dissolution of liquid microdroplets into a receptor liquid has also been quantified by Poesio *et al*. by recording images of a hexadecane droplet in an acetone receptor phase, and measuring the droplet radius over time.[27]

This paper presents a series of investigations to quantify monomer transfer within a thermosetting epoxy-amine PMP system currently used in the agrochemical industry for pesticide encapsulation.[28] The transfer of jeffamine D230 out of RDGE epoxy resin carrier was measured potentiometrically via MEMED using a micro pH-electrode.[29, 30]

The transfer of the epoxide into the aqueous phase and the nature of curing at the liquid-liquid interface would also be expected to influence PMP morphology. To further our understanding of these processes, experiments were devised to probe the effect of temperature and solution composition on the dissolution of an RDGE droplet. A glass capilliary connected to a syringe pump was used to generate RDGE droplets in either deionised water or a jeffamine D230 solution with temperature control. Time lapse microscopy was then used to monitor the change in RDGE droplet size as a function of both solution and temperature. Droplet radius versus time profiles were obtained from which initial flux values were determined by utilising image analysis to measure droplet dissolution.[31]

Materials and Methods

Chemicals. RDGE (Sigma-Aldrich) and jeffamine D230 (Alfa Chemicals) were mixed at a 2:1 molar ratio for MEMED. Pure RDGE and an aqueous solution of 5 mM jeffamine D230 was used in the optical dissolution experiments. Electrochemical characterisation of Au electrodes after construction was carried out using 500 µM trimethyl(ferrocenylmethyl) ammonium hexafluorophosphate ($FcTMA^+PF_6^-$) solution containing 0.1 M KNO_3 (99%, Sigma-Aldrich). $FcTMA^+PF_6^-$ was synthesized in-house as described previously,[32] following the metathesis reaction between ferrocenylmethyltrimethylammonium iodide and silver hexafluorophosphate. Electrochemical characterisation of the Au microelectrodes after iridium oxide deposition

was carried out using 0.1 M H_2SO_4 (95%, Fisher Chemical) containing 0.1 M KNO_3. Aqueous solutions of jeffamine D230 with a known pH were used to calibrate the iridium-oxide coated Au microelectrodes. The iridium oxide solution used for the electrodeposition was prepared as described in the literature[33] and stored at 4 °C between uses. All reagents were used as received, and all solutions and the aqueous receptor phases were prepared with deionised water (Milli-Q, Millipore, 18.2 MΩ cm resistivity at 25 °C).

Figure 2. Schematic of the experimental setup used for MEMED of a 2:1 RDGE/ jeffamine D230 droplet expanding towards a pH-sensitive IrOx-coated Au microelectrode in water.

MEMED Apparatus and Procedure. A schematic of the experimental setup used is shown in Figure 2. The set up for MEMED has been described previously.[25] In this study, droplets of RDGE containing jeffamine D230 (in a 2:1 molar ratio) were grown from a tapered glass capilliary (internal diameter ca. 100 µm, fabrication described previously)[25] into a receptor phase of deionised water. A pH-sensitive microelectrode (see Supporting Information sections S1 and S2 for construction and characterisation) was placed in the receptor phase opposite the tapered glass capilliary, held in the PTFE base using wax. The flow of the RDGE/jeffamine D230 organic phase was controlled by a high precision syringe pump (KD Scientific), with a flow rate of 800 µL/h to ensure fast refreshment of the interface. Potentiometric detection was used to measure the transfer of jeffamine D230, inferred as a change in pH, into the aqueous phase as the droplet expanded. Time stamped

photographs of the expanding droplet were taken at intervals in the range of 20-300 ms using a PixeLINK© B700 camera. These were related to the response of the pH sensitive probe to its distance from the droplet, from which the time dependent concentration profiles were obtained. All measurements were made at ambient temperature (21 °C ± 1 °C).

Potentiometric measurements were carried out using a two electrode set up, consisting of the previously calibrated pH-sensitive microelectrode and a saturated calomel electrode (SCE). The potential was measured using a purpose-built voltage follower. An external data acquisition card (NI USB-6211, National Instruments, Austin, TX) connected to a desktop PC was used to record open circuit potential (OCP)-time data.

Software written in LabVIEW© (National Instruments) recorded the OCP every 35-40 ms and ensured that photographs were taken during the same time period. Photographs were later analysed in MATLAB© to measure the electrode-droplet separation as a function of time and thus directly relate the OCP to the distance between the droplet and the electrode. Previous electrode calibration data was then used to convert OCP measurements to pH and hence the concentration of jeffamine D230 in the aqueous phase (see Figure S2, Supporting Information section S2).

Figure 3. (a) Experimental setup for time lapse microscopy of an RDGE droplet held in water or a 5 mM jeffamine D230 solution heated to different temperatures using a circulating water jacket. (b) Photographs of an RDGE droplet in (i) water or (ii) jeffamine D230 heated to 50°.

Apparatus and Procedure for Monitoring Epoxide Droplet Dissolution. A schematic of the experimental setup is shown in Figure 3a. A circulating water jacketed vessel was filled with either deionised water or an aqueous solution of 5 mM jeffamine D230

and heated to 40, 50 or 70 °C. RDGE droplets of ca. 800 µm diameter were formed at the tip of a fine glass capilliary (internal diameter ca. 40 µm) immersed in the aqueous phase. The capilliary was connected via a Luer syringe needle attached to PTFE tubing (Cole-Palmer) to a 10 mL syringe (BD Plastipak) containing 5 mL of RDGE. A syringe pump (KD Scientific) using a flow rate of 400 µL/h was used to hold the syringe in place and push RDGE to the tip of the glass capilliary. A PixeLINK© B700 camera was then used to take photographs of the droplet every 20 seconds for 2000 seconds as dissolution took place, as demonstrated in Figure 3b. These photographs were analysed in MATLAB© to calculate the change in droplet diameter over time and thus the dissolution flux of RDGE from the droplet into the aqueous phase.

Construction of Glass Capillaries. A borosilicate glass capilliary (2.0 mm outer diameter, Harvard Apparatus Limited) was heated at a point a third along its length in order to bend it by an angle of ca. 90 °. It was then heated further along the long end to bend the capilliary back on itself (ca. 90 °), thus forming a U-shape. Another smaller borosilicate glass capilliary (1.0 mm outer diameter, Harvard Apparatus Limited) was heat pulled to form a fine tip then shortened. This was then inserted and sealed into the shorter end of the U-shaped capilliary using epoxy adhesive (Araldite®).

Simulations and Modelling. All finite element method (FEM) modelling was performed using Comsol Multiphysics 4.4 (Comsol AB, Sweden) using a PC equipped with an Intel core i3-3220 and 4 GB of RAM, running 64 bit Windows 7. Full details can be found in Supporting Information section S3.

Jeffamine D230 Transfer (MEMED). A one-dimensional FEM model was developed to simulate the transfer of the amine into the aqueous phase as a droplet expanded towards a fixed point (the sensor electrode). The boundary condition was a flux on the organic/aqueous

interface, with no depletion in the droplet which was reasonable. The simulations produced amine concentration profiles from the droplet into the aqueous phase with the flux adjusted to fit experimental data.

Results and Discussion

Measuring Amine Transfer from an Expanding Droplet into Aqueous Solution. The concentration of jeffamine D230 adjacent to the moving droplet surface was calculated from pH (potentiometric) measurements taken during MEMED. Experiments were carried out using a 2:1 molar ratio of RDGE and jeffamine D230 as the organic phase and deionised water as the receptor phase. Raw experimental data for jeffamine D230 transport studied by potentiometric detection is shown in Figure 4a. Shown alongside are photographs taken at various times during the potentiometric-time transient. This indicates that the voltage measured remains essentially constant until the surface of the drop is very close to the probe electrode, between positions (iii) and (iv), when the potentiometric response changes rapidly with time in a manner indicating a rapid increase in pH. Note that a key feature of this type of pH electrode is its rapid response time[30] so that it can faithfully follow the pH gradient in the boundary layer near the droplet.

Figure 4. (a) A typical potentiometric transient recorded at an IrOx-coated Au microelectrode during the transfer of jeffamine D230 into the aqueous phase from a growing 2:1 RDGE/jeffamine D230 drop surface. Images (i)-(iv) show the relative positions of the capilliary, drop and IrOx-coated Au microelectrode and correspond to the points indicated on the transient. (b) Calculated pH versus electrode-droplet separation. (c) Calculated Jeffamine

D230 concentration versus electrode-droplet separation (●). Alongside is the theoretical concentration versus separation profile (■) generated using a moving plane model built in COMSOL software (see section S3 of Supporting Information).

Analysis of time lapse photographs such as those in Figure 4(a) (i)-(iv) allowed the electrode-droplet separation to be deduced as a function of time. Potentiometric measurements were converted to corresponding pH values using a calibration curve such as that shown in Figure S2 (see Supporting Information, section S2). Figure 4(b) shows a typical resulting pH versus electrode-droplet separation profile. As the droplet interface approached within a sufficiently close distance to the probe electrode (electrode-droplet separation ≤ 100 μm), the pH increase corresponds to a local jeffamine D230 concentration increase. pH measurements were then converted into concentration of jeffamine D230, with a typical profile shown in Figure 4c. The concentration of a weak base can be calculated from the pH of the solution so long as the pKa is known, which was calculated to be ~9.4 for jeffamine D230. This is achieved using the Henderson-Hasselbalch equation:

$$pOH = pK_b + \log\frac{\left[BH^+\right]}{\left[B\right]} \quad (1)$$

FEM modelling as described in Supporting Information, section S3, generated theoretical concentration profiles that matched well with experimental data for an interfacial flux value of 17.5±5.1 nmol cm^{-2} s^{-1}. This highlights how MEMED provides new quantitative information on this initial liquid reactive interface system.

Dependence of Epoxide Droplet Dissolution on Temperature and Composition of Solution. As shown in Figure 3, RDGE droplet dissolution was characterised by forming similar sized RDGE droplets (c.a. 800 μm diameter) in a vessel containing either water or aqueous jeffamine D230 solution immersed in a controlled temperature cell and using time-lapse microscopy to monitor the change in size. Image analysis of droplet size by time-lapse microscopy was then used to determine the radius of the RDGE droplet as a function of time. Typical results of this analysis can be seen in Figure 5, which clearly shows how varying the temperature of the aqueous solution will affect the rate of RDGE droplet dissolution. It appears that higher temperatures lead to a faster initial droplet dissolution rate. However, it is apparent that over time the rate decreases dramatically, indicating a shutting off of dissolution. Moreover, the cessation of dissolution occurs earlier the higher the aqueous receptor solution temperature. An explanation is that as RDGE dissolves, it may react with water and homopolymerise. As the epoxide polymerises at the liquid-liquid interface, or near the interface, it adsorbs to the droplet surface, resulting in a barrier layer that impedes dissolution. This hypothesis is supported by the work of Qu *et al.*, who have shown that water at higher temperatures can promote the ring-opening of epoxides by acting as a modest acid catalyst.[34] Ring-opening of epoxides will form alcohol groups, which have been shown to react with adjacent epoxide groups under hot water conditions to form polyethers.[35]

Figure 5. Averaged radius versus time profiles (3-5 runs) for an RDGE droplet held in water (■) or 5 mM jeffamine D230 aqueous solution (●) heated to 40, 50 and 70 °C.

RDGE droplet dissolution into aqueous jeffamine D230 solution (5 mM) is also influenced by temperature (see Figure 5). The initial rate of RDGE droplet dissolution (until droplet reaches 350 μm radius) appears to increase as the temperature is increased; however this rate decreases in a temperature-dependent manner, qualitatively consistent to the results

for droplet dissolution in water. It is also clear that in the temperature range 50 °C – 70 °C, the jeffamine D230 has a significant impact on the dissolution rate. This is reasonable because hot water-promoted ring-opening of epoxides has been shown to be enhanced in the presence of amines in comparison to without.[34] The dissolution profiles for RDGE droplets in the presence of jeffamine D230 and water at 40° remain closely similar, indicating sluggish like curing or homopolymerisation on the timescale considered.

In an attempt to quantify droplet dissolution kinetics, the droplet radius calculated from image analysis of each frame in the time-lapse was used to calculated droplet volume and surface area. Given the molar volume of RDGE of 183.67 cm^3 mol^{-1}, this then readily allowed initial fluxes in the two media and at the range of temperatures to be calculated. These are shown in Table 1, which compares the average initial flux of RDGE out of droplets in water and aqueous jeffamine D230. Average initial dissolution flux values increase dramatically with increasing temperature for RDGE droplets in water, but at equivalent temperatures in aqueous jeffamine D230 they are comparatively lower. It can also be noted that as the temperature increases, the difference between the initial flux of RDGE from a droplet in water and the initial flux of RDGE from a droplet in an aqueous jeffamine D230 solution is much more significant. The higher the temperature, the more the RDGE-jeffamine D230 curing reaction rate is enhanced and thus the earlier the blocking of dissolution occurs.

Table 1. Initial flux (with standard error) of RDGE into the aqueous phase from droplets held in either water or aqueous jeffamine D230 heated to different temperatures.

	40 °C	**50 °C**	**70 °C**
Initial flux in water / nmol cm^{-2}	37.6±5.9	86.4±4.7	234.0±3.5

s^{-1}			
Initial flux in 5 mM jeffamine D230 / nmol cm^{-2} s^{-1}	35.1±0.9	52.5±3.9	68.0±6.2

Conclusions

Interfacial physicochemical processes that take place during an emulsion polymerisation reaction have been studied using microelectrochemical measurements at expanding droplets and time-lapse microscopy. Local pH measurements recorded with microelectrochemical measurements at expanding droplets of 2:1 molar ratio droplets of resorcinol diglycidyl ether and jeffamine D230 and subsequent finite element method modelling have quantified the kinetics of jeffamine D230 transfer from the organic phase into the aqueous phase, a process about which little was known previously.

Time-lapse microscopy of resorcinol diglycidyl ether droplets held in either deionised water or an aqueous solution of jeffamine D230, at different temperatures, has been used to monitor the effect of solution and temperature on resorcinol diglycidyl ether dissolution into the aqueous phase and the interfacial curing reaction of the amine and the epoxide. Interestingly, without amine, resorcinol diglycidyl ether appears to homopolymerise in water at higher temperatures, but the addition of jeffamine D230 introduces the amine-curing reaction that at elevated temperatures is faster than the resorcinol diglycidyl ether homopolymerisation reaction. With increasing resorcinol diglycidyl ether flux values at higher temperatures, we expect higher concentrations of resorcinol diglycidyl ether to be present in the aqueous phase adjacent to the oil phase droplet. Alongside the influence of

thermal effects on the kinetics and the fast transfer of the jeffamine D230 into the aqueous phase, these effects have the potential to influence the density of microcapsules produced by this technology. For example, with curing close to the liquid-liquid interface and in the aqueous phase, it can be postulated that oligomers formed from the curing reaction will cross-link at the interface, which could lead to polymeric microparticles with a heterogeneous density. This would influence the extent of active ingredient inclusion and the rate of release upon polymeric microparticle wall decomposition. The studies herein provide vital chemical insight on monomer transfer and reactivity that should be valuable for deeper understanding of the consequences for polymeric microparticle morphology. It is envisioned that the techniques applied in this study can be utilised to examine other emulsion polymerisation systems currently used for polymeric microparticle synthesis.

Acknowledgements. EO would like to thank EPSRC and Syngenta UK for an iCASE award. The authors thank Dr Maxim Joseph for helpful discussions on FEM modelling, Dr Kim McKelvey for design of the data acquisition program in LabVIEW©, Dr Eleni Bitziou for helpful discussions on data analysis, Dr Sophie Kinnear for helpful MATLAB© discussions, Dr Alexander Parker for his contribution to the iridium oxide preparation, and Dr Jonathan Newland for photography of experiments.

References

[1] A.G. Volkov, Liquid interfaces in chemical, biological and pharmaceutical applications, CRC Press2001.

[2] A. Asakawa, M. Unoki, T. Hirono, T. Takayanagi, Waterborne fluoropolymers for paint use, J. Fluorine Chem. 104(1) (2000) 47-51.

[3] Y. Zhao, W. Zhang, L.-p. Liao, S.-j. Wang, W.-j. Li, Self-healing coatings containing microcapsule, Appl. Surf. Sci. 258(6) (2012) 1915-1918.

[4] L. Zhang, Y. Cao, L. Wang, L. Shao, Y. Bai, Polyacrylate emulsion containing IBOMA for removable pressure sensitive adhesives, J. Appl. Polym. Sci. 133(3) (2016) n/a-n/a.

[5] S. Freiberg, X. Zhu, Polymer microspheres for controlled drug release, Int. J. Pharm. 282(1) (2004) 1-18.

[6] C. Wang, Q. Ge, D. Ting, D. Nguyen, H.-R. Shen, J. Chen, H.N. Eisen, J. Heller, R. Langer, D. Putnam, Molecularly engineered poly(ortho ester) microspheres for enhanced delivery of DNA vaccines, Nat Mater 3(3) (2004) 190-196.

[7] B. Hack, H. Egger, J. Uhlemann, M. Henriet, W. Wirth, A.W.P. Vermeer, D.G. Duff, Advanced Agrochemical Formulations through Encapsulation Strategies?, Chem. Ing. Tech. 84(3) (2012) 223-234.

[8] P.J. Dowding, R. Atkin, B. Vincent, P. Bouillot, Oil Core−Polymer Shell Microcapsules Prepared by Internal Phase Separation from Emulsion Droplets. I. Characterization and Release Rates for Microcapsules with Polystyrene Shells, Langmuir 20(26) (2004) 11374-11379.

[9] K. Eggers, D. Szopinski, G.A. Luinstra, Thermo-Responsive Microcapsules Based on Guar Gum Derivatives, Macromolecular Symposia 346(1) (2014) 32-35.

[10] B.P. Binks, M. Kirkland, Interfacial structure of solid-stabilised emulsions studied by scanning electron microscopy, PCCP 4(15) (2002) 3727-3733.

[11] C.C. Riccardi, H.E. Adabbo, R.J.J. Williams, Curing Reaction of Epoxy Resins with Diamines, J. Appl. Polym. Sci. 29 (1984) 2481-2492.

[12] A. Moroni, J. Mijovic, E.M. Pearce, C.C. Foun, Cure kinetics of epoxy resins and aromatic diamines, J. Appl. Polym. Sci. 32(2) (1986) 3761-3773.

[13] R. Mezzenga, L. Boogh, J.A.E. Månson, A thermodynamic model for thermoset polymer blends with reactive modifiers, J. Polym. Sci., Part B: Polym. Phys. 38(14) (2000) 1893-1902.

[14] C. Byrne, G. Hagnauer, N. Schneider, Effects of variation in composition and temperature on the amine cure of an epoxy resin model system, Polym. Compos. 4(4) (1983) 206-213.

[15] A.N. Netravali, R.E. Fornes, R.D. Gilbert, J.D. Memory, Effects of water sorption at different temperatures on permanent changes in an epoxy, J. Appl. Polym. Sci. 30(4) (1985) 1573-1578.

[16] P. Johncock, Effect of absorbed water on undercured epoxy/amine thermosets, J. Appl. Polym. Sci. 41(3-4) (1990) 613-618.

[17] S. Choi, A.P. Janisse, C. Liu, E.P. Douglas, Effect of water addition on the cure kinetics of an epoxy-amine thermoset, J. Polym. Sci., Part A: Polym. Chem. 49(21) (2011) 4650-4659.

[18] C.J. Slevin, P.R. Unwin, Measurement of Liquid/Liquid Interfacial Kinetics by Directly Probing the Concentration Profiles at Expanding Droplets, Langmuir 13(18) (1997) 4799-4803.

[19] J. Zhang, P.R. Unwin, Potential Dependence of Electron-Transfer Rates at the Interface between Two Immiscible Electrolyte Solutions: Reduction of 7,7,8,8-Tetracyanoquinodimethane in 1,2-Dichloroethane by Aqueous Ferrocyanide Studied with Microelectrochemical Techniques, The Journal of Physical Chemistry B 104(10) (1999) 2341-2347.

[20] J. Zhang, P.R. Unwin, Microelectrochemical measurements at expanding droplets (MEMED): investigtaion of cupric ion stripping kinetics in a two-hase oil/water system, Phys. Chem. Chem. Phys. 2 (2000) 1267-1271.

[21] J. Zhang, C.J. Slevin, L. Murtomäki, K. Kontturi, D.E. Williams, P.R. Unwin, Microelectrochemical Measurements at Expanding Droplets: Effect of Surfactant Adsorption on Electron Transfer Kinetics at Liquid/Liquid Interfaces, Langmuir 17(3) (2001) 821-827.

[22] J. Zhang, P.R. Unwin, Microelectrochemical measurements of electron transfer rates at the interface between two immicible electrolyte soutions: Potential dependence of the ferro/ferricyanide-7,7,8,8-tetracyanoquinodimethane(TCNQ)/TCNQ- system, Phys. Chem. Chem. Phys. 4 (2002) 3820-3827.

[23] J. Zhang, P.R. Unwin, Kinetics of IrCl62- Ion Transfer across the Water/1,2-Dichloroethane Interface and the Effect of a Phospholipid Monolayer, Langmuir 18(6) (2002) 2313-2318.

[24] J. Zhang, J.H. Atherton, P.R. Unwin, Investigation of the Kinetics and Mechanism of Acid chloride hydrolysis in an Oil/Water System Using Microelectrochemical Measurements at Expanding Droplets (MEMED), Langmuir 20 (2004) 1864-1870.

[25] C.J. Slevin, P.R. Unwin, Microelectrochemical Measurements at Expanding Droplets (MEMED): Mass-Transport Characterization and Assessment of Amperometric and Potentiometric Electrodes as Concentration Boundary Layer Probes of Liquid/Liquid Interfaces, Langmuir 15(21) (1999) 7361-7371.

[26] P.B. Duncan, D. Needham, Microdroplet Dissolution into a Second-Phase Solvent Using a Micropipet Technique: Test of the Epstein-Plesset Model for an Aniline-Water System, Langmuir 22 (2006) 4190-4197.

[27] P. Poesio, G.P. Beretta, T. Thorsen, Dissolution of a Liquid Microdroplet in a Nonideal Liquid-Liquid Mixture Far from Thermodynamic Equilibrium, Phys. Rev. Lett. 103(6) (2009) 064501.

[28] S. Kim, J.D. Fowler, Formulation, U.S. Patent Application 14/353,947, (2014).

[29] W. Olthuis, M.A.M. Robben, P. Bergveld, M. Bos, W.E. van der Linden, pH sensor properties of electrochemically grown iridium oxide, Sensors and Actuators B: Chemical 2(4) (1990) 247-256.

[30] B.P. Nadappuram, K. McKelvey, R. Al Botros, A.W. Colburn, P.R. Unwin, Fabrication and Characterization of Dual Function Nanoscale pH-Scanning Ion Conductance Microscopy (SICM) Probes for High Resolution pH Mapping, Anal. Chem. 85(17) (2013) 8070-8074.

[31] P. Poesio, G. Beretta, T. Thorsen, Dissolution of a Liquid Microdroplet in a Nonideal Liquid-Liquid Mixture Far from Thermodynamic Equilibrium, Phys. Rev. Lett. 103(6) (2009).

[32] S.G. Lemay, D.M. van den Broek, A.J. Storm, D. Krapf, R.M. Smeets, H.A. Heering, C. Dekker, Lithographically fabricated nanopore-based electrodes for electrochemistry, Anal. Chem. 77(6) (2005) 1911-1915.

[33] T.L. Read, E. Bitziou, M.B. Joseph, J.V. Macpherson, In Situ Control of Local pH Using a Boron Doped Diamond Ring Disk Electrode: Optimizing Heavy Metal (Mercury) Detection, Anal. Chem. 86(1) (2013) 367-371.

[34] Z. Wang, Y. Cui, Z. Xu, J. Qu, Hot Water-Promoted Ring-Opening of Epoxides and Aziridines by Water and Other Nucleophiles, J. Org. Chem. 73 (2008) 2270-2274.

[35] C.J. Morten, J.A. Byers, A.R. Van Dyke, I. Vilotijevic, T.F. Jamison, The development of endo-selective epoxide-opening cascades in water, Chem. Soc. Rev. 38(11) (2009) 3175-3192.

Supporting Information

Interfacial Kinetics in a Model Emulsion Polymerisation System Using Microelectrochemical Measurements at Expanding Droplets (MEMED) and Time Lapse Microscopy

Elizabeth E. Oseland,[†] Anita Rea,[‡] Martine de Heer, [‡] Jeffrey Fowler, [‡] and Patrick R. Unwin*,[†]

[†]*Department of Chemistry, University of Warwick, Coventry CV4 7AL, United Kingdom*

[‡]*Jealott's Hill International Research Centre, Bracknell, Berkshire RG42 6EY, United Kingdom*

*Email: P.R.Unwin@warwick.ac.uk; Telephone: +44 24 76524112

Table of Contents

S1 – Construction of pH-sensitive microelectrodes for MEMED. A 2 mm diameter borosilicate glass tube (Harvard apparatus) was pulled using a home-built heating coil to form a 100-200 µm diameter tip at one end. A 15 mm long piece of 75 µm diameter Au wire (Goodfellow Ltd, Cambridge, UK) coated in PTFE was attached alongside the end of a 15 cm long, 250 µm diameter copper wire using conductive silver paint, with around half the length of the Au wire protruding past the tip of the copper wire. The wire was then carefully pushed through the glass tube until the Au wire was sticking out of the narrow end of the tube. The end of the copper wire protruding from the glass tube was then wrapped around the end of the glass tube to keep the wire in place, leaving a straight section at the end to which an connection could be made. The ends of the glass tube were then sealed around the wire using epoxy adhesive (Araldite®). Electrodes were tested against a standard calomel electrode (SCE) in a 500 µM $FcTMA^+$ solution containing 0.1 M KNO_3 using cyclic voltammetry (CV) (scan speed 10 mV/s). The steady-state limiting current response for $FcTMA^+$ oxidation was used to calculate the microelectrode radius:[1]

$$i_{\text{lim}} = 4nFDC^*a \qquad \text{(S1)}$$

where n is the number of moles of electrons transferred, F is Faraday's constant (96485 C mol^{-1}) D is the diffusion coefficient (cm^2 s^{-1}), C^* is the bulk concentration (mol cm^{-3}) and a is the radius of the microelectrode (cm).

Iridium Oxide Film Electrodeposition. Iridium oxide film formation on the electrode surface is controlled by the reaction:[2, 3]

$$[Ir(COO)_2(OH)_4]^{2-}{}_{(aq)} + 2OH^- \rightarrow [Ir(OH)_2 \bullet 2H_2O]_{(s)} + 2CO_2 + 2e^- \qquad \text{(S1)}$$

A three electrode system consisting of a Ag|AgCl wire reference electrode, a platinum counter electrode and a fabricated Au wire working electrode (sensor to be functionalised) was assembled in the iridium solution. Anodic deposition was carried out using a potentiostat (CHI800B, CH Instruments Inc.) connected to a desktop computer, with a potential of 0.8 V applied for 180 seconds. The electrodes were then left overnight in deionised water to hydrate, as this has been shown to stabilise the pH response.[4] A current-time (*I-t*) curve for the anodic electrodeposition of iridium oxide is shown in Figure S1.

Figure S1. An *I-t* curve for the anodic electrodeposition of iridium oxide onto an Au microelectrode.

S2 – Characterisation of pH-sensitive microelectrodes for MEMED. Cyclic voltammetry of Au microelectrodes in 0.1 M H_2SO_4 (scan rate 0.1 V s^{-1}) was carried out before and after electrochemical deposition to confirm iridium oxide film formation, as shown in Figure S2.

Figure S2. Cyclic voltammograms at a 75 µm diameter Au wire electrode before (-) and after (-) electrodeposition of iridium oxide; 0.1 M H_2SO_4, scan rate 0.1 V s^{-1}. Inset shows potential-pH calibration of a typical IrOx-coated Au microelectrode.

The anodic peak at 0.75 V corresponds to the oxidation of Ir(III) to Ir(IV) and the cathodic peak corresponds to the reduction of Ir(IV) back to Ir(III). Similar peak potentials for the oxidation of Ir(III) in H_2SO_4 have been reported in the literature.[5, 6]

The pH-sensitive potentiometric response of iridium oxide electrodes is governed by the redox process:[2, 3]

$$2\left[IrO_2\left(OH\right)_{2-x}\bullet\left(2+x\right)H_2O\right]^{(2-x)-}+\left(3-2_x\right)H^+ + 2e^- \longleftrightarrow \left[Ir_2O_3\left(OH\right)_3\bullet 3H_2O\right]+3H_2O \quad \text{(S2)}$$

This process means that iridium oxide electrodes often exhibit a super-Nernstian pH response, with calibration slopes reported ranging from -59 to -90 mV per pH unit.[7] A typical calibration plot for a pH-sensitive Au microelectrode is shown in Figure S2 inset. Calibration slopes of -68 mV/pH ± 2 mV were obtained over pH range 7.5-11. Previous pH probe calibrations in the literature have indicated that the pH response of iridium oxide films can be affected by the constituents of the solution in which they are placed.[8] Thus, to ensure that the potentiometric response of the electrode would adequately reflect the pH change of water as jeffamine D230 transfers into the aqueous phase, pH microelectrode probe calibration was carried out using aqueous solutions of jeffamine D230. The pH of the aqueous jeffamine D230 calibration solutions ranged between pH 7.75 to 11.06 (measured using a conventional glass pH electrode, S20 SevenEasy™ pH, Mettler Toldeo). The open circuit potential (OCP) of the pH-sensitive microelectrode versus an SCE was measured for 100 seconds in each solution in order of increasing basicity. This was then reversed and repeated to provide at least three measurements at each pH and to ensure that the pH probe was stable.

S3 - FEM simulation of jeffamine D230 transfer from an expanding droplet. Previous MEMED studies have solved mass-transport problems for symmetrically expanding

spheres[9-11], however as the droplets in this study do not expand in a symmetrical manner it was instead assumed that treating the drop surface approaching the electrode as a moving plane would be a more accurate approximation. The convective-diffusion equation which describes this case and is used as the basis of this model is:[12]

$$\frac{\partial c_x}{\partial t} = D_i \frac{\partial^2 c_x}{\partial r^2} - 2v_r \frac{\partial^2 c_x}{\partial r} \tag{S3}$$

where D_x is the diffusion coefficient ($m^2\ s^{-1}$), c_x is the concentration of jeffamine D230 (mol m^{-3}), t is time (s) and r is the spherical coordinate measured from the centre of the drop (m). The variable v_r is the convective velocity ($m\ s^{-1}$) of the moving surface of the expanding drop and is given by:

$$v_r = \frac{q}{4\pi}\left(\frac{1}{r^2} - \frac{1}{r_0^2}\right) \tag{S4}$$

where q is the volume flow rate ($m^3\ s^{-1}$), which was modified in the model to ensure that the total drop time, $t_{d,}$ correlated with the total drop time recorded experimentally. The (time-dependent) drop radius, $r_{o,}$ was calculated using the equation:

$$r_0 = \left(\frac{3q}{4\pi}\right)^{1/3} t^{1/3} \tag{S5}$$

where t is any time less than $t_{d.}$ The mass-transport of the species of interest, described by equation S3, was solved for the domain within the model where $r > r_o$, which describes the aqueous phase outside the droplet. Mass-transport within the droplet was not considered, as

depletion and hence diffusional effects within the droplet are negligible under these experimental conditions. The boundary condition placed on this domain can be described as:

$$r \longrightarrow \infty : c = 0 \tag{S6}$$

The surface of the drop during MEMED can be described using the following boundary condition:

$$r = r_0 : j = -D_x \frac{\partial c_x}{\partial r} \tag{S7}$$

where j is the interfacial flux of the species of interest (mol m^{-2} s^{-1}). Diffusion coefficient, $D_{x,}$ was calculated using the Wilke-Chang equation, which can be found in Supporting Information section S4.[13]

To quantify the flux of jeffamine D230 transfer from the droplet into the aqueous phase, a finite element method (FEM) model was built to simulate mass-transport from an expanding droplet as a function of time. The three domains simulated are shown in Figure S3. The uni-axis spatial geometry was built consisting of a line from 0 mm (P_a) to 5 mm (P_d), with a fixed point at 0.682 mm (P_c) to simulate the position of the electrode in terms of distance from the centre of the droplet. Another point at 1 nm (P_b) was built to simulate the surface of the droplet; during the simulation this was displaced in accordance with the droplet expansion equation S5. The flux value at P_b was fixed to achieve the best correlation between experimental data with the model.

Figure S3. Schematic of the 1D model built in COMSOL to simulate the local concentration change at a fixed point (the electrode; Pc) as a droplet (Pa→Pb) expands towards it.

The droplet (domain D1) was defined as the distance between P_a and $P_{b.}$ The convective-diffusion equation S3 was solved only for domains D2 and D3, which represents the distance between the droplet surface and the electrode and the distance between the electrode and the edge of the simulation geometry, respectively. The diffusion coefficient of jeffamine D230 was set to 4.4 x 10^{-6} cm^2 s^{-1}. The initial concentration of jeffamine D230 in domains D2 and D3 was set as zero.

A mesh was built with an element length of 10^{-11} m at point $P_{b;}$ the remaining domains were meshed continuously at a growth rate of 1.01x per element from this point until they reached a maximum size of 1 μm at the edge of the simulation domain. Free deformation of meshing within all domains allowed for mesh displacement of point P_b in accordance with equation S5. The mesh consisted of 24354 elements and was solved in a time-dependent manner for the duration of droplet experiments using the MUMPS solver within COMSOL.

S4 – Wilke-Chang estimation of diffusion coefficients. Diffusion coefficients for jeffamine D230 were predicted using the Wilke-Chang formula:[13]

$$D = \frac{7.4\times10^{-8}\left(\phi\times M_B\right)^{\frac{1}{2}}T}{\mu\times V_A^{\,0.6}} \qquad \text{(S8)}$$

where D is the diffusion coefficient (cm^2 s^{-1}), $\emptyset$ is the association parameter for the solvent, M_B is the molecular weight of the solvent (g mol^{-1}), μ is the viscosity of the solvent (cP), V_A is the molecular volume of the molecule (cm^3 mol^{-1}) calculated by the LeBas method[14] and T is temperature (K). This approach is appropriate in that it will give diffusion coefficient values for jeffamine D230 in water, however it should be noted that this formula is known to

have an error of around 13%.[15]. The values used and calculated for jeffamine D230 using the Wilke-Chang estimation are shown in Table S1.

Table S1. Parameters used and diffusion coefficient calculated for jeffamine D230 in water at 21 °C using the Wilke-Chang estimation.

Parameter	$\emptyset$	M_B / g mol^{-1}	μ / cP	V_A / cm^3 mol^{-1}	T / K	D / cm^2 s^{-1}
Value at 21 °C	2.6	18	1.002	296.4	294.15	4.89 x 10^{-6}

References

[1] A.J. Bard, L.R. Faulkner, Electrochemical methods: principles and applications, Electrochemical Methods: Principles and Applications (2001) 386-428.

[2] B.P. Nadappuram, K. McKelvey, R. Al Botros, A.W. Colburn, P.R. Unwin, Fabrication and Characterization of Dual Function Nanoscale pH-Scanning Ion Conductance Microscopy (SICM) Probes for High Resolution pH Mapping, Anal. Chem. 85(17) (2013) 8070-8074.

[3] E. Bitziou, D. O'Hare, B.A. Patel, Simultaneous Detection of pH Changes and Histamine Release from Oxyntic Glands in Isolated Stomach, Anal. Chem. 80(22) (2008) 8733-8740.

[4] L.D. Burke, D.P. Whelan, A voltammetric investigation of the charge storage reactions of hydrous iridium oxide layers, Journal of Electroanalytical Chemistry and Interfacial Electrochemistry 162(1–2) (1984) 121-141.

[5] D.O. Wipf, F. Ge, Microscopic Measurement of pH with Iridium Oxide Microelectrodes, Anal. Chem. 72 (2000) 4921-4927.

[6] J.E. Baur, T.W. Spaine, Electrochemical deposition of iridium (IV) oxide from alkaline solutions of iridium(III) oxide, J. Electroanal. Chem. 443(2) (1998) 208-216.

[7] H.A. Elsen, C.F. Monson, M. Majda, Effects of Electrodeposition Conditions and Protocol on the Properties of Iridium Oxide pH Sensor Electrodes, J. Electrochem. Soc. 156(1) (2009) F1-F6.

[8] P. Steegstra, E. Ahlberg, Influence of oxidation state on the pH dependence of hydrous iridium oxide films, Electrochim. Acta 76(0) (2012) 26-33.

[9] C.J. Slevin, P.R. Unwin, Measurement of Liquid/Liquid Interfacial Kinetics by Directly Probing the Concentration Profiles at Expanding Droplets, Langmuir 13(18) (1997) 4799-4803.

[10] J. Zhang, C.J. Slevin, L. Murtomäki, K. Kontturi, D.E. Williams, P.R. Unwin, Microelectrochemical Measurements at Expanding Droplets: Effect of Surfactant Adsorption on Electron Transfer Kinetics at Liquid/Liquid Interfaces, Langmuir 17(3) (2001) 821-827.

[11] J. Zhang, J.H. Atherton, P.R. Unwin, Investigation of the Kinetics and Mechanism of Acid chloride hydrolysis in an Oil/Water System Using Microelectrochemical Measurements at Expanding Droplets (MEMED), Langmuir 20 (2004) 1864-1870.

[12] C.J. Slevin, P.R. Unwin, Microelectrochemical Measurements at Expanding Droplets (MEMED): Mass-Transport Characterization and Assessment of Amperometric and Potentiometric Electrodes as Concentration Boundary Layer Probes of Liquid/Liquid Interfaces, Langmuir 15(21) (1999) 7361-7371.

[13] C.R. Wilke, P. Chang, Correlation of Diffusion Coefficients in Dilute Solutions, A. I. Ch. E. Journal (1955) 264-270.

[14] J.S. Gulliver, Introduction to chemical transport in the environment, Cambridge University Press2007.

[15] R. Sitaraman, S.H. Ibrahim, N.R. Kuloor, A Generalized Equation for Diffusion in Liquids, Journal of Chemical & Engineering Data 8(2) (1963) 198-201.